Wilson, P.A., Lyle, M., and Firth, J.V. (Eds.)
Proceedings of the Ocean Drilling Program, Scientific Results Volume 199

11. Data Report: High-Resolution Mineralogy for Leg 199 Based on Reflectance Spectroscopy and Physical Properties[1]

Michael D. Vanden Berg[2,3] and Richard D. Jarrard[2]

ABSTRACT

During Ocean Drilling Program Leg 199 in the equatorial Pacific, visible and near-infrared spectroscopy (VNIS) was used to measure the reflectance spectra (350–2500 nm) of 1343 sediment samples. Reflectance spectra were also measured for a suite of 60 samples of known mineralogy, thereby providing a local ground-truth calibration of spectral features to percentages of calcite, opal, smectite, and illite. The associated algorithm was used to calculate mineral percentages from the 1343 spectra. Using multiple regression and VNIS mineralogy, multisensor track physical properties and light spectroscopy data were then converted into continuous high-resolution mineralogy logs.

INTRODUCTION

A latitudinal transect of Cenozoic sediments, particularly Paleogene sequences, was collected during Leg 199 of the Ocean Drilling Program (ODP) in order to study the paleoceanography and paleoclimate of the last 55 m.y. (Lyle, Wilson, Janecek, et al., 2002). The Pacific plate has steadily drifted northward throughout Cenozoic time, transporting Paleogene biogenic sediments, which were deposited under the high-productivity equatorial belt, into the red clay zone of extremely slow sediment accumulation (van Andel, 1974). Consequently, the central tropical North Pacific Ocean is an ideal region in which to sample shal-

[1] Vanden Berg, M.D., and Jarrard, R.D., 2006. Data report: High-resolution mineralogy for Leg 199 based on reflectance spectroscopy and physical properties. *In* Wilson, P.A., Lyle, M., and Firth, J.V. (Eds.), *Proc. ODP, Sci. Results,* 199, 1–23 [Online]. Available from World Wide Web: <http://www-odp.tamu.edu/publications/199_SR/VOLUME/CHAPTERS/203.PDF>. [Cited YYYY-MM-DD]
[2] Department of Geology and Geophysics, University of Utah, Salt Lake City UT 84112, USA. Correspondence author: **jarrard@earth.utah.edu**
[3] Present address: Utah Geological Survey, Energy and Minerals Section, 1594 West North Temple, Salt Lake City UT 84114, USA.

Initial receipt: 30 December 2003
Acceptance: 2 February 2006
Web publication: 26 July 2006
Ms 199SR-203

lowly buried Paleogene sequences of equatorially deposited biogenic sediments. The thin Neogene cover of red clay allowed the Paleogene sediments to be reached by advanced piston coring and extended core barrel drilling, which achieve much higher core recovery than rotary drilling. Eight sites were drilled during Leg 199, seven of which were located on a north–south transect along 56- to 57-Ma crust. The eighth site (Site 1218) was drilled on 40-Ma crust to collect a well-preserved Eocene/Oligocene boundary sequence. This site was located in shallower water because of its eastern location, resulting in higher rates of carbonate accumulation.

This study is the first to use visible and near-infrared spectroscopy (VNIS) to determine high-resolution mineralogy. VNIS-based mineralogy for each Leg 199 site provides a ground-truth for the conversion of multisensor track (MST) and light spectroscopy logs to continuous mineralogy logs. These concentration logs of calcium carbonate (derived almost entirely from nannofossils), biogenic opal (derived mainly from radiolarians), and terrigenous materials (almost exclusively wind-deposited clays) provide a foundation for the calculation of high-resolution mass accumulation rates for each component (Vanden Berg and Jarrard, 2004).

SPECTROSCOPY-BASED MINERALOGY

Previous Work

The ultimate goal of all sediment spectroscopy techniques is to provide accurate qualitative or quantitative estimates of sediment composition. Many studies have shown that different marine sediment types have distinctive spectral features within the visible and very near infrared region of the electromagnetic spectrum. Mix et al. (1992, 1995) developed and used a prototype split-core analysis track (SCAT) for automated core scanning of reflectance (wavelength = 455–945 nm) during ODP Leg 138. Their goal was to estimate biogenic calcite, biogenic opal, and nonbiogenic contents from recovered cores. Their estimates were best for biogenic calcite, but opal and nonbiogenic material were not always distinguished reliably. A revised SCAT instrument with an improved signal-to-noise ratio and wider frequency band (250–950 nm vs. earlier 455–945 nm) was used during ODP Legs 154, 162, and 167 (Harris et al., 1997; Shipboard Scientific Party, 1997; Ortiz et al., 1999b).

Starting with Leg 154, shipboard core scanning with the Minolta spectrophotometer (400–700 nm) became a routine measurement. ODP scientists used these data as a proxy for many different minerals, mainly calcite (e.g., Shipboard Scientific Party, 1995). Balsam et al. (1999) evaluated the use of visible light (400–700 nm) spectroscopy, or optical lightness, as a proxy for the carbonate content of marine sediments in five Atlantic piston cores and ODP Hole 997A. Their carbonate estimates were good, but they warned that optical lightness is strongly affected by the composition of the noncarbonate fraction, such as clay. Balsam and Deaton (1996) used 250- to 850-nm spectra to estimate concentrations of carbonate, opal, and organic carbon in various Atlantic piston cores and at ODP Site 847 (East Pacific Rise). They found that the character of downcore changes in mineralogy was well determined but systematic offsets were sometimes evident for individual mineral concentrations. Additional visible-range spectral research, summarized by

Balsam and Damuth (2000), includes use of the slope of the reflectance curve to estimate chlorite and organic carbon (Balsam and Deaton, 1991) or hematite and goethite (Deaton and Balsam, 1991) and factor analysis to extract indicators of up to five components (Balsam and Damuth, 2000).

VNIS Technique

In contrast to the various studies mentioned above, we measured broader-band, 350- to 2500-nm spectra for the visible and expanded near-infrared region of the electromagnetic spectrum (Vanden Berg and Jarrard, 2002). The additional spectral information found in the expanded near-infrared region greatly improves identification of paleoclimatically significant minerals (Fig. F1), yet this frequency band had previously been used mainly for remote sensing and economic geology studies (Goetz et al., 1983; Clark and Roush, 1984; Clark et al., 1990, 2003). By using local ground-truth to calibrate specific spectral responses, we developed algorithms that could be used to rapidly calculate concentrations of calcite and opal, as well as the two main terrigenous minerals, smectite and illite.

F1. Reflectance spectra, p. 9.

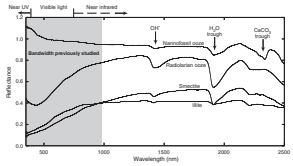

The eight Leg 199 sites were sampled at a spacing of ~0.75 m, and then all 1343 samples were dried and crushed to powder. Each sample was illuminated with a quartz halogen light at a near-vertical angle, and the reflected visible and near-infrared spectrum (350–2500 nm) was recorded at 1-nm spacing and 3- to 10-nm resolution with an ASD FieldSpec Pro FR portable spectroradiometer (Vanden Berg and Jarrard, 2002).

To calibrate the VNIS response to local mineralogy, we use geochemical analyses of samples from the same region. An alternative approach is to use mixes of pure mineral standards. However, VNIS response is sensitive to both grain size and—especially for clays—subtle compositional variations (Clark et al., 1990). An additional advantage of using local ground-truth samples is that spectral features sensitive to other minor components (e.g., organic matter) can be identified and avoided.

Sixty local ground-truth samples were chosen from several sites in the Leg 199 area: Deep Sea Drilling Project (DSDP) Site 162 (Leg 16), four Leg 199 site survey cores (EW9709), and samples from three Leg 199 sites (Table T1). The first set of ground-truth data consisted of 14 samples from DSDP Site 162 (14°N, 140°W), ranging in depth from 0.9 to 150.0 meters below seafloor (mbsf). These samples were analyzed by Olivarez-Lyle and Lyle (2002) for calcite and opal concentrations. X-ray diffraction (XRD) analyses indicate that smectite is the dominant clay mineral throughout Site 162 (Zemmels, 1973). The second set consists of 35 samples taken from four EW9709 cores, the site survey cores for ODP Leg 199: EW9709-3PC (21°N, 139°W), EW9709-7PC (8°N, 135°W), EW9709-12PC (5°N, 140°W), and EW9709-21GC (26°N, 147°W). Olivarez-Lyle and Lyle (2002) determined calcite and opal concentrations for these samples. The dominant clay mineral (illite or smectite) was identified subjectively by VNIS interpretation. In order to increase the range of ground-truth compositions, 11 samples from Leg 199 Sites 1215, 1218, and 1219 were added to the ground-truth sample suite. These included three samples containing 100% illite, three samples with moderate calcite and smectite concentrations, and seven samples with high calcite concentrations. Calcite percentages were measured during the cruise by coulometer (Lyle, Wilson, Janecek, et al., 2002). The clay mineralogy was derived from location in the core and spectral

T1. Mineralogical ground-truth data, p. 20.

characteristics. Clay percentages were calculated by assuming that opal + calcite + clay = 100%. The terrigenous component of all ground-truth samples commonly includes minor amounts of quartz and other clay species, but we only refer to the dominant clay mineral.

The next step in the VNIS technique was to evaluate which spectral features are sensitive to mineral concentrations. We began by calculating 11 spectral features that may be indicative of concentration of any of the four components. For example, depth of the 1900-nm water trough, relative to adjacent peaks, might be sensitive to concentrations of opal and smectite, both of which contain structural water. Our focus centered on the 1400- and 1900-nm trough depths as well as subtle differences in spectral character in the 2000- to 2500-nm range because of substantial differences among the four components at these wavelengths (Fig. **F1**). Eight spectral features were selected and confirmed to be potentially useful based on individual cross-plots of spectral feature vs. mineral concentration. Some of these features have a nonlinear relationship to mineral concentrations; these nonlinearities were reduced via transforms (e.g., raising to a power, taking the square root).

Onboard during Leg 199, mineralogy was calculated from VNIS spectra (Lyle, Wilson, Janecek, et al., 2002) by using the algorithm of Vanden Berg and Jarrard (2002) based on multiple regression of spectral features on ground-truth mineralogy followed by matrix inversion. Postcruise analyses, however, demonstrated that significantly better agreement between predicted and ground-truth mineralogy could be obtained by using stepwise multiple regression, with each ground-truth mineral percentage as dependent variable and with the suite of spectral features as independent variables.

When multiple regression is used to determine transforms relating mineral concentration to geophysical properties, a potential pitfall is that some predictive variables are merely chance (spurious) correlations. One test for this problem is to split the ground-truth data set into calibration and verification portions (e.g., Mix et al., 1992). Another approach is to reduce the number of independent variables via principal component analysis (PCA) prior to the mineralogy regression (e.g., Handwerger and Jarrard, 2003). Our approach was to begin the statistical analyses with a relatively small number of potential independent variables and then use stepwise multiple regression to confine the final predictive equations to only the most significant terms.

Rather than use a simple four-mineral (calcite, opal, smectite, and illite) solution for all sediments, we apply one set of equations to the upper clay intervals, which contain primarily smectite and illite, and a second set of equations for intervals containing mixtures of calcite, opal, and smectite (Table **T2**). This method reduces two problems encountered in the original shipboard calculations: overestimation of calcite in light-colored clays and prediction of opal in smectite-rich zones. Our mineral calculation equations sometimes predict slightly negative concentrations for a mineral component. These negative concentrations were converted to zero, and then concentrations of all components were adjusted to a total of 100%. Table **T1** and Figure **F2** compare known mineral concentrations to VNIS-predicted mineral concentrations. The correlation coefficients range from a high of 0.99 for illite to a low of 0.95 for the three-mineral smectite solution. We note, however, that the determinations of relative percentages of smectite vs. illite are much less accurate than their excellent correlation coefficients suggest because of the paucity of intermediate mixes (Fig. **F2B**).

T2. Spectral features, p. 22.

F2. VNIS-predicted and ground-truth mineralogy, p. 10.

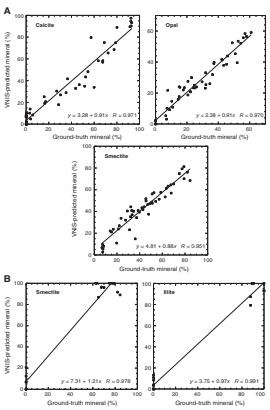

Figure F3 displays the calculated mineral concentrations plotted vs. depth for each site drilled during Leg 199 (Site 1216 is omitted because it contains only terrigenous materials); these data are tabulated in Vanden Berg (2003). Lithologic columns and units are also included, as well as first-order ages. These figures illustrate that the VNIS-mineralogy data indicate major changes in lithology as well as more subtle mineral variations. The dominant clay mineral is smectite. Illite is present, but it is restricted to the upper 15 m of core (Fig. F4). The accuracy of VNIS-based calcite concentrations can also be evaluated by comparison to independent coulometer calcite concentrations (Fig. F5). The correlation between the two data sets is very good (VNIS-predicted calcite is ±5% of coulometer calcite) despite the fact that the compared samples were sometimes up to 2 cm apart. Calcite was measured by coulometer during Leg 199 at a sample spacing of ~4.6 m, whereas VNIS-based calcite concentrations were measured at a spacing of ~0.75 m.

CONVERSION OF CONTINUOUS-CORE PHYSICAL PROPERTIES INTO MINERALOGY LOGS

A variety of techniques have been employed to calculate mineralogy from high-resolution physical property logs. For example, Mayer (1991), Herbert and Mayer (1991), and Hagelberg et al. (1995) used polynomial regression to estimate carbonate contents from MST bulk density. DeMenocal et al. (1992) used multiple regression of downhole logs to calculate concentrations of opal, carbonate, and terrigenous materials. Balsam and Deaton (1991, 1996), Schneider et al. (1995), Ortiz et al. (1999a), and Balsam et al. (1999) used multiple or linear regression of reflectance spectral features to calculate carbonate and various clay minerals. PCA has also been applied to MST and downhole logs for calculation of carbonate and clay percentages (Handwerger and Jarrard, 2003).

Our calculations of mineralogy from physical properties differ from previous studies in two significant respects. First, we quantify four components, whereas most previous analyses distinguished only two components (but see deMenocal et al., 1992; Balsam and Damuth, 2000). Second, our VNIS-based mineralogy provides an order of magnitude more ground-truth data than are usually available to calibrate the conversion from physical properties to mineralogy.

Continuous-core physical properties included in this conversion were the mineralogy-dependent MST logs—gamma-ray attenuation bulk density and magnetic susceptibility—plus four reflectance logs from the ODP Digital Core Imaging System (Minolta core scanner): total reflectance measured over the entire visible range (400–700 nm) (L*), reflectance in the red (a*) and blue (b*) regions, and a ratio of red to blue (a*/b*) (Lyle, Wilson, Janecek, et al., 2002). The MST compressional wave velocity log was not used because of its dependence on porosity instead of mineralogy and because of reliability problems, and the natural gamma ray log was excluded because of its low sample frequency and low signal-to-noise ratio. For each site, the MST/Minolta logs were edited to remove spurious values associated with severely disturbed core. The optimum equations for converting the MST/Minolta logs into mineralogy were determined via stepwise multiple regression, with VNIS-based estimates of carbonate, opal, or terrigenous fraction as

F3. VNIS-based and MST/MR mineralogy, p. 11.

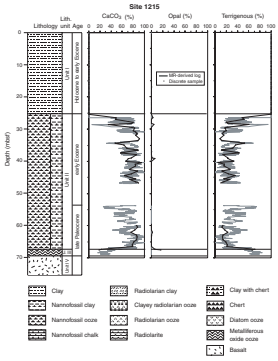

F4. VNIS-based clay mineralogy, p. 18.

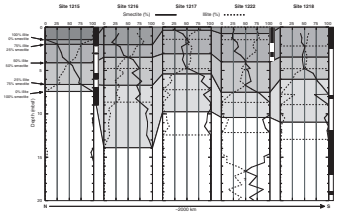

F5. VNIS-based calcite concentrations, p. 19.

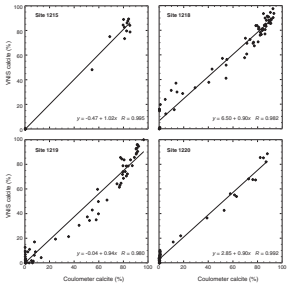

the dependent variable and the suite of MST/Minolta logs as independent variables.

Deeper sites were split into two or three depth intervals, separated at changes in coring method (advanced piston core vs. extended core barrel) or major lithologic changes for separate multiple regressions. This technique worked remarkably well, often resulting in correlation coefficients between 0.90 and 0.99 (Table T3). An alternative to multiple regression is PCA or factor analysis. This technique was used by Balsam and Damuth (2000) to estimate five mineral components from light spectroscopy data and by Handwerger and Jarrard (in press) for calculation of carbonate and clay percentages from MST and downhole logs. We found that PCA was also successful for estimating mineralogy of Leg 199 sites, but multiple regression was superior.

Figure F3 compares the VNIS ground-truth mineralogy (discrete samples) with the MST/Minolta-based mineralogy logs for all Leg 199 sites except Site 1216, which contained only terrigenous materials.

T3. MR analyses, p. 23.

ACKNOWLEDGMENTS

We thank W.H. Busch for shipboard advice and collaboration, S. O'Connell for manuscript review, and M.W. Lyle for help throughout this project. This research used data provided by the Ocean Drilling Program (ODP). ODP is sponsored by the U.S. National Science Foundation and participating countries under management of Joint Oceanographic Institutions, Inc. Funding for this research was provided to Vanden Berg and Jarrard by the U.S. Science Support Program.

REFERENCES

Balsam, W.L., and Damuth, J.E., 2000. Further investigations of shipboard vs. shore-based spectral data: implications for interpreting Leg 164 sediment composition. *In* Paull, C.K., Matsumoto, R., Wallace, P.J., and Dillon, W.P. (Eds.), *Proc. ODP, Sci. Results,* 164, 101–112 [Online]. Available from World Wide Web: <**http://www-odp.tamu.edu/publications/164_SR/VOLUME/CHAPTERS/SR164_31.PDF**>.

Balsam, W.L., and Deaton, B.C., 1991. Sediment dispersal in the Atlantic Ocean: evaluation by visible light spectra. *Rev. Aquat. Sci.,* 4:411–447.

Balsam, W.L., and Deaton, B.C., 1996. Determining the composition of late Quaternary marine sediments from NUV, VIS, and NIR diffuse reflectance spectra. *Mar. Geol.,* 134:31–55. **doi:10.1016/0025-3227(96)00037-0**

Balsam, W.L., Deaton, B.C., and Damuth, J.E., 1999. Evaluating optical lightness as a proxy for carbonate content in marine sediment cores. *Mar. Geol.,* 161:141–153. **doi:10.1016/S0025-3227(99)00037-7**

Clark, R.N., King, T.V.V., Klejwa, M., Swayze, G.A., and Vergo, N., 1990. High spectral resolution reflectance spectroscopy of minerals. *J. Geophys. Res., [Solid Earth Planets],* 95(8):12653–12680.

Clark, R.N., and Roush, T.L., 1984. Reflectance spectroscopy: quantitative analysis techniques for remote sensing applications. *J. Geophys. Res.,* 89:6329–6340.

Clark, R.N., Swayze, G.A., Livo, K.E., Kokaly, R.F., Sutley, S.J., Dalton, J.B., McDougal, R.R., and Gent, C.A., 2003. Imaging spectroscopy: Earth and planetary remote sensing with the USGS tetracorder and expert systems. *J. Geophys. Res.,* 108. **doi:10.1029/2002JE001847**

Deaton, B.C., and Balsam, W.L., 1991. Visible spectroscopy: a rapid method for determining hematite and goethite concentrations in geological materials. *J. Sediment. Petrol.,* 61:628–632.

deMenocal, P.B., Bristow, J.F., and Stein, R., 1992. Paleoclimatic applications of downhole logs: Pliocene–Pleistocene results from Hole 798B, Sea of Japan. *In* Pisciotto, K.A., Ingle, J.C., Jr., von Breymann, M.T., Barron, J., et al., *Proc. ODP, Sci. Results,* 127/128 (Pt. 1): College Station, TX (Ocean Drilling Program), 393–406.

Goetz, A.F.H., Barrett, N.R., and Rowan, L.C., 1983. Remote sensing for exploration: an overview. *Econ. Geol.,* 78:573–590.

Hagelberg, T.K., Pisias, N.G., Mayer, L.A., Shackleton, N.J., and Mix, A.C., 1995. Spatial and temporal variability of late Neogene equatorial Pacific carbonate: Leg 138. *In* Pisias, N.G., Mayer, L.A., Janecek, T.R., Palmer-Julson, A., and van Andel, T.H. (Eds.), *Proc. ODP, Sci Results,* 138: College Station, TX (Ocean Drilling Program), 321–336.

Handwerger, D.A., and Jarrard, R.D., 2003. Neogene changes in Southern Ocean sedimentation based on mass accumulation rates at four continental margins. *Paleoceanography,* 18. **doi:10.1029/2002PA000850**

Harris, S.E., Mix, A.C., and King, T., 1997. Biogenic and terrigenous sedimentation at Ceara Rise, western tropical Atlantic, supports Pliocene–Pleistocene deep-water linkage between hemispheres. *In* Shackleton, N.J., Curry, W.B., Richter, C., and Bralower, T.J. (Eds.), *Proc. ODP, Sci. Results,* 154: College Station, TX (Ocean Drilling Program), 331–345. [**PDF**]

Herbert, T.D., and Mayer, L.A., 1991. Long climatic time series from sediment physical property measurements. *J. Sediment. Petrol.,* 61:1089–1108.

Lyle, M.W., Wilson, P.A., Janecek, T.R., et al., 2002. *Proc. ODP, Init. Repts.,* 199 [CD-ROM]. Available from: Ocean Drilling Program, Texas A&M University, College Station TX 77845-9547, USA. [**HTML**]

Mayer, L., 1991. Extraction of high-resolution carbonate data for paleoclimate reconstruction. *Nature (London, U. K.),* 352:148–151. **doi:10.1038/352148a0**

Mix, A.C., Harris, S.E., and Janecek, T.R., 1995. Estimating lithology from nonintrusive reflectance spectra: Leg 138. *In* Pisias, N.G., Mayer, L.A., Janecek, T.R., Palmer-

Julson, A., and van Andel, T.H. (Eds.), *Proc. ODP, Sci. Results,* 138: College Station, TX (Ocean Drilling Program), 413–427.

Mix, A.C., Rugh, W., Pisias, N.G., Veirs, S., Leg 138 Shipboard Sedimentologists (Hagelberg, T., Hovan, S., Kemp, A., Leinen, M., Levitan, M., Ravelo, C.), and Leg 138 Scientific Party, 1992. Color reflectance spectroscopy: a tool for rapid characterization of deep-sea sediments. *In* Mayer, L., Pisias, N., Janecek, T., et al., *Proc. ODP, Init. Repts.,* 138 (Pt. 1): College Station, TX (Ocean Drilling Program), 67–77.

Olivarez Lyle, A., and Lyle, M.W., 2002. Determination of biogenic opal in pelagic marine sediments: a simple method revisited. *In* Lyle, M., Wilson, P.A., Janecek, T.R., et al., *Proc. ODP, Init. Repts.,* 199, 1–21 [CD-ROM]. Available from: Ocean Drilling Program, Texas A&M University, College Station TX 77845-9547, USA. [**HTML**]

Ortiz, J., Mix, A.C., Harris, S., and O'Connell, S., 1999. Diffuse spectral reflectance as a proxy for percent carbonate content in North Atlantic sediments. *Paleoceanography,* 14(2):171–186. **doi:10.1029/1998PA900021**

Ortiz, J.D., O'Connell, S., and Mix, A., 1999. Data report: Spectral reflectance observations from recovered sediments. *In* Raymo, M.E., Jansen, E., Blum, P., and Herbert, T.D. (Eds.), 1999. *Proc. ODP, Sci. Results,* 162: College Station, TX (Ocean Drilling Program), 259–264. [**HTML**]

Schneider, R.R., Cramp, A., Damuth, J.E., Hiscott, R.N., Kowsmann, R.O., Lopez, M., Nanayama, F., Normark, W.R., and Shipboard Scientific Party, 1995. Color-reflectance measurements obtained from Leg 155 cores. *In* Flood, R.D., Piper, D.J.W., Klaus, A., et al., *Proc. ODP, Init. Repts.,* 155: College Station, TX (Ocean Drilling Program), 697–700.

Shipboard Scientific Party, 1995. Leg 154 synthesis. *In* Curry, W.B., Shackleton, N.J., Richter, C., et al., *Proc. ODP, Init. Repts.,* 154: College Station, TX (Ocean Drilling Program), 421–442.

Shipboard Scientific Party, 1997. Explanatory notes. *In* Lyle, M., Koizumi, I., Richter, C., et al., *Proc. ODP, Init. Repts.,* 167, 15–39 [Online]. Available from World Wide Web: <**http://www-odp.tamu.edu/publications/167_IR/CHAP_02.PDF**>.

van Andel, T.H., 1974. Cenozoic migration of the Pacific plate, northward shift of the axis of deposition, and paleobathymetry of the central equatorial Pacific. *Geology,* 2:507–510. **doi:10.1130/0091-7613(1974)2<507:CMOTPP>2.0.CO;2**

Vanden Berg, M.D., and Jarrard, R.D, 2002. Determination of equatorial Pacific mineralogy using light absorption spectroscopy. *In* Lyle, M.W., Wilson, P.A., Janecek, T.R., et al., *Proc. ODP, Init. Repts.,* 199, 1–20 [CD-ROM]. Available from: Ocean Drilling Program, Texas A&M University, College Station TX 77845-9547, USA. [**HTML**]

Vanden Berg, M.D., and Jarrard, R D., 2004. Cenozoic mass accumulation rates in the equatorial Pacific based on high-resolution mineralogy of Ocean Drilling Program Leg 199. *Paleoceanography,* 19:PA2021. **doi:10.1029/2003PA000928**

Vanden Berg, M.D., 2003. The use of light absorption spectroscopy as a mineral identification tool: implications for the study of Cenozoic paleoclimate [M.S. thesis]. Univ. Utah, Salt Lake City.

Zemmels, I., 1973. X-ray mineralogy studies—Leg 16. *In* van Andel, T.H., Heath, G.R., et. al., *Init. Repts. DSDP,* 16: Washington (U.S. Govt. Printing Office), 529–572.

Figure F1. Reflectance spectra from the four climatically sensitive minerals involved in this study. Reflectance of 1.0 corresponds to that of a white reference calibration plate. Previous marine sediment studies only measured the visible bandwidth in the highlighted area. Additional spectral information present in the expanded near-infrared region greatly improves identification of minerals affected by paleoclimatic changes.

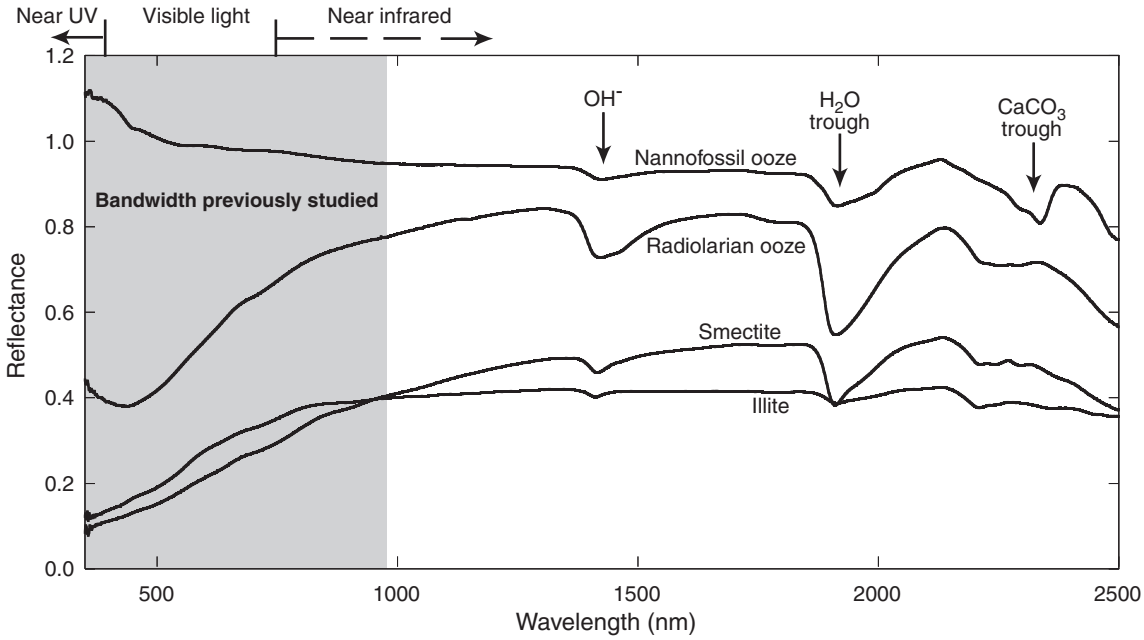

Figure F2. Cross-plots comparing visible and near-infrared spectroscopy (VNIS)-predicted mineralogy with ground-truth mineralogy for the postcruise calibration method. Both the (**A**) three mineral and (**B**) two (clay) mineral solutions are shown along with regression line equations and correlation coefficients (R).

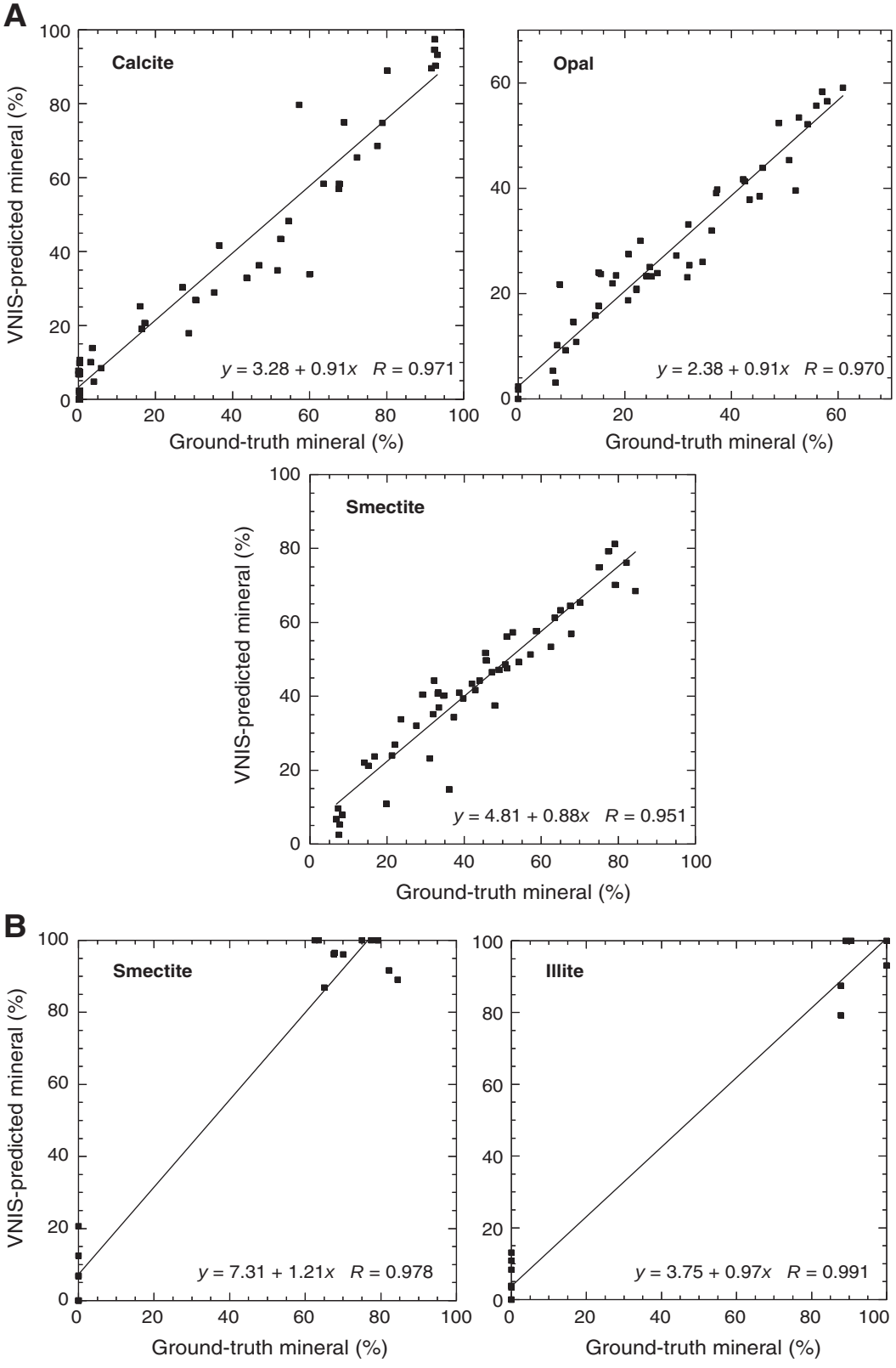

Figure F3. Comparison of VNIS-based mineralogy (discrete samples) and MST/Minolta-based multiple regression (MR) mineralogy, both plotted vs. depth for all Leg 199 sites (Site 1216 not included because it contains only terrigenous materials). Lithologic columns (from Lyle, Wilson, Janecek, et al., 2002) and units are also included, as well as first-order age data. (Continued on next six pages.)

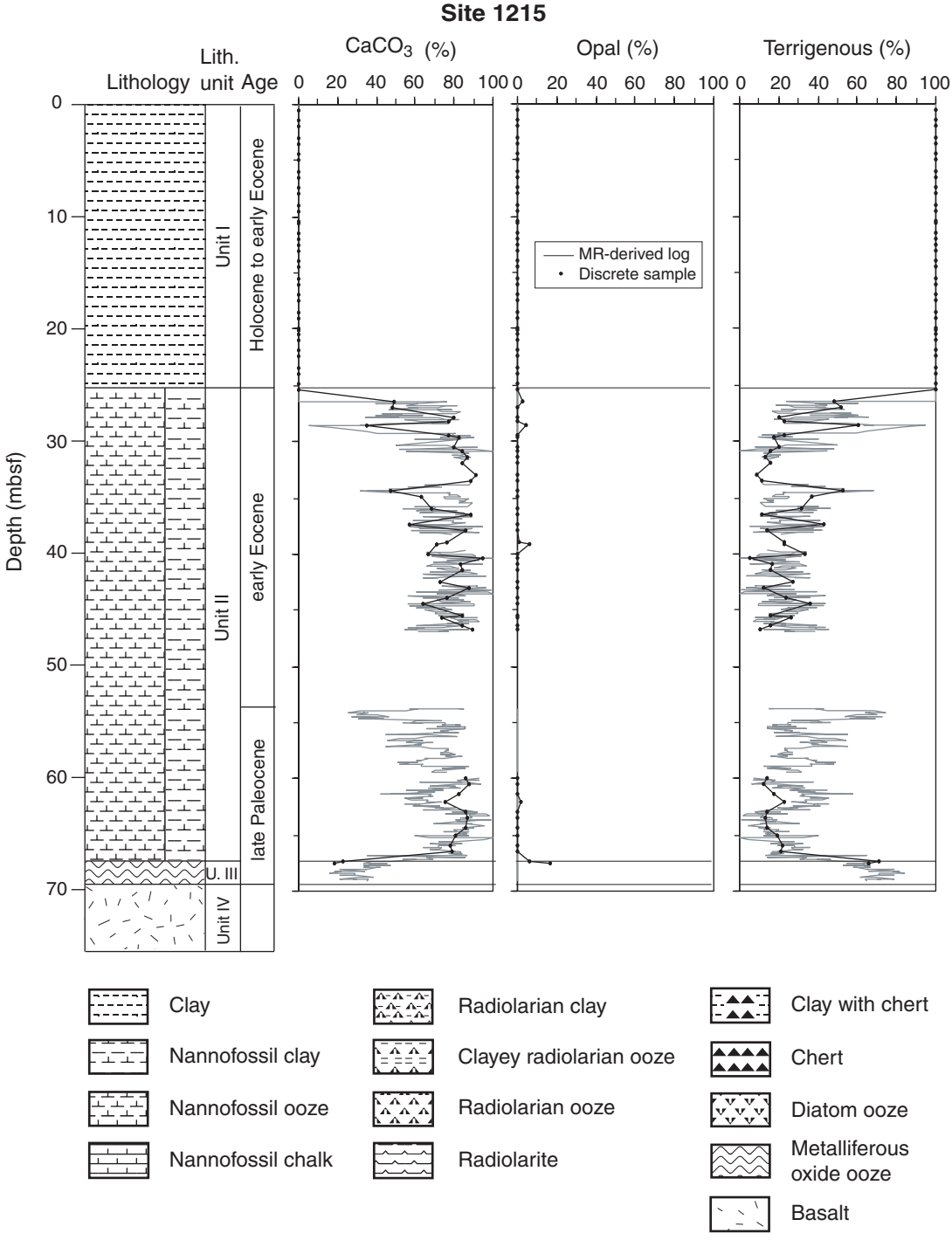

Figure F3 (continued).

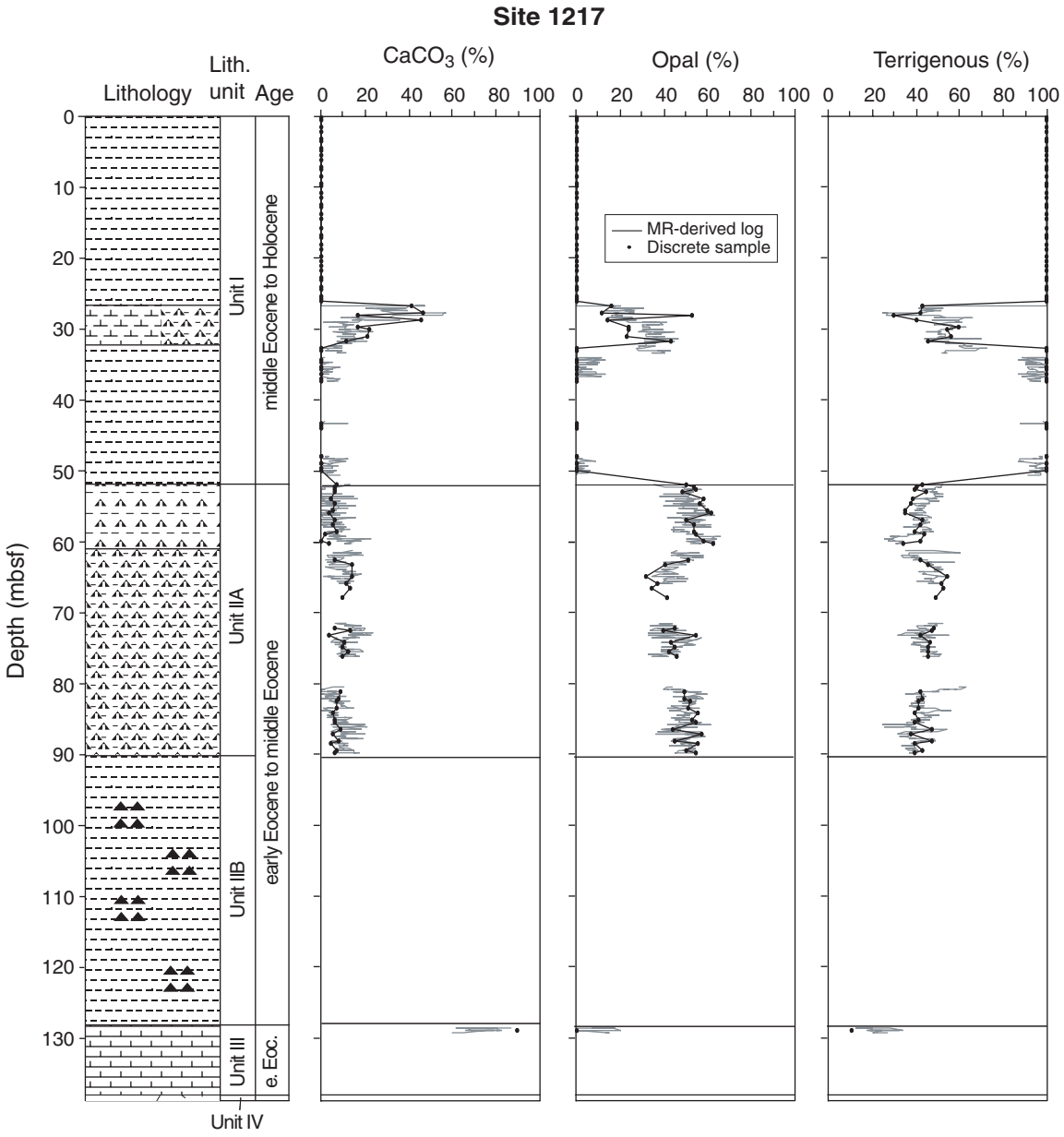

Figure F3 (continued).

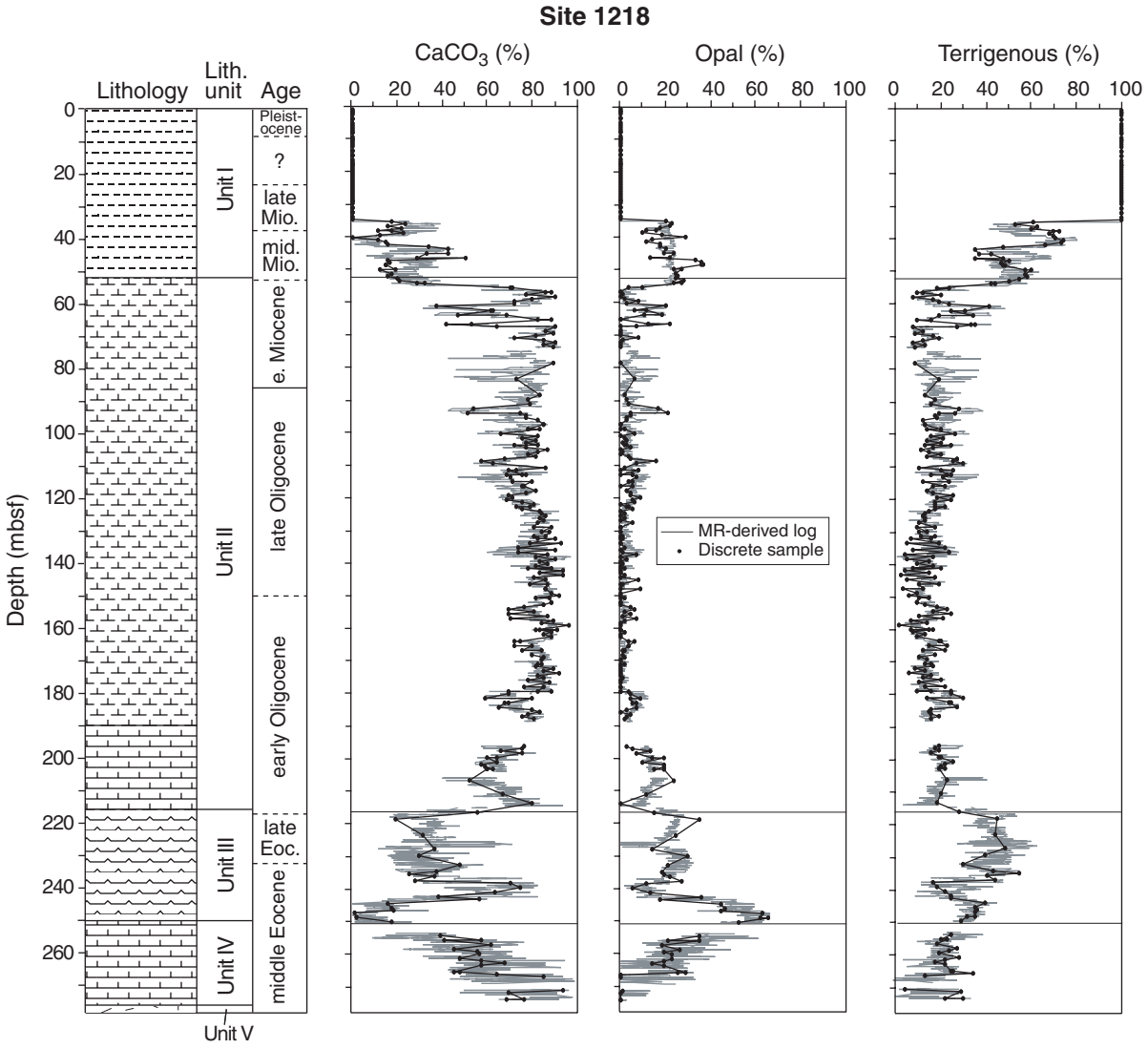

Figure F3 (continued).

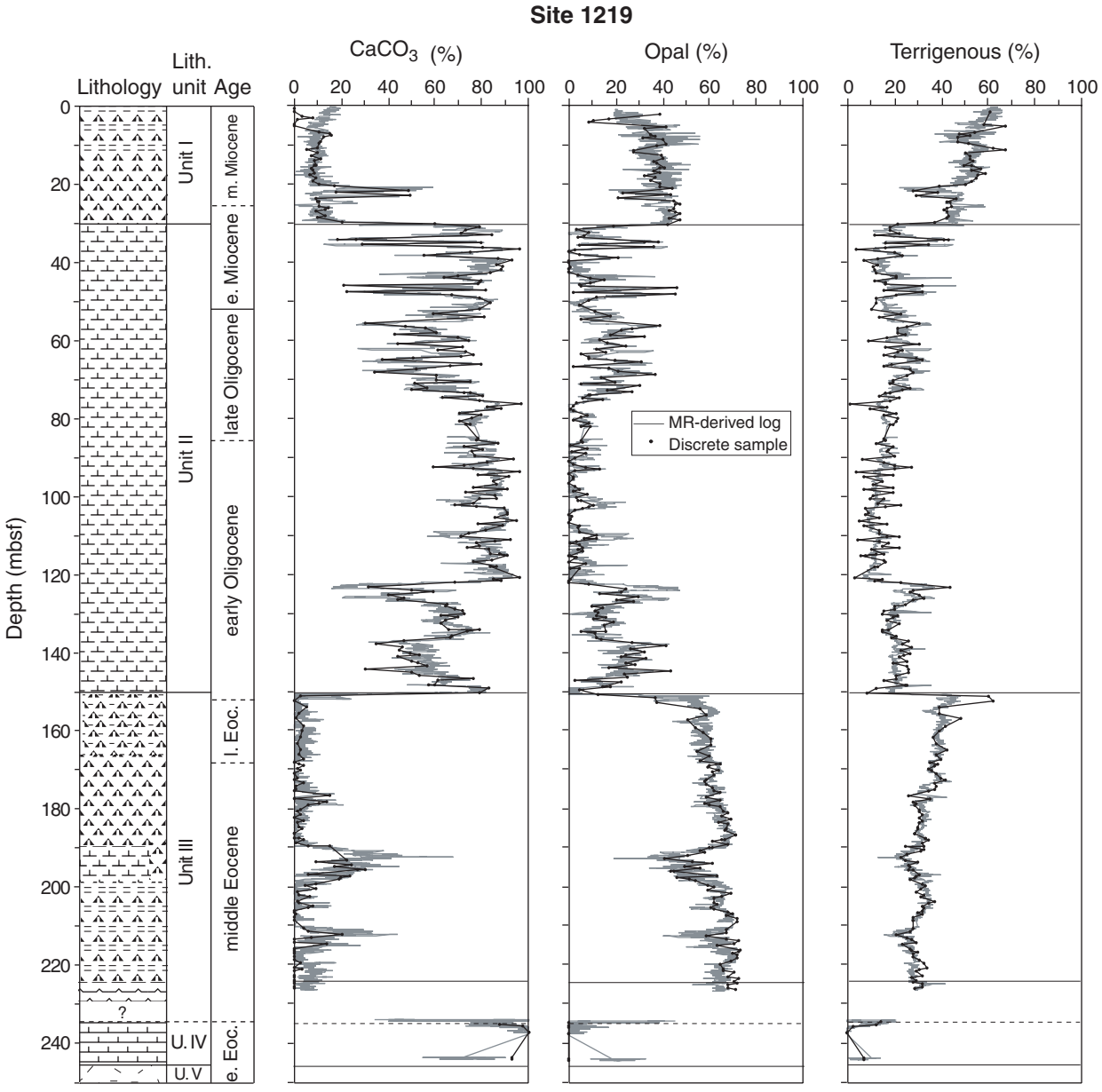

Figure F3 (continued).

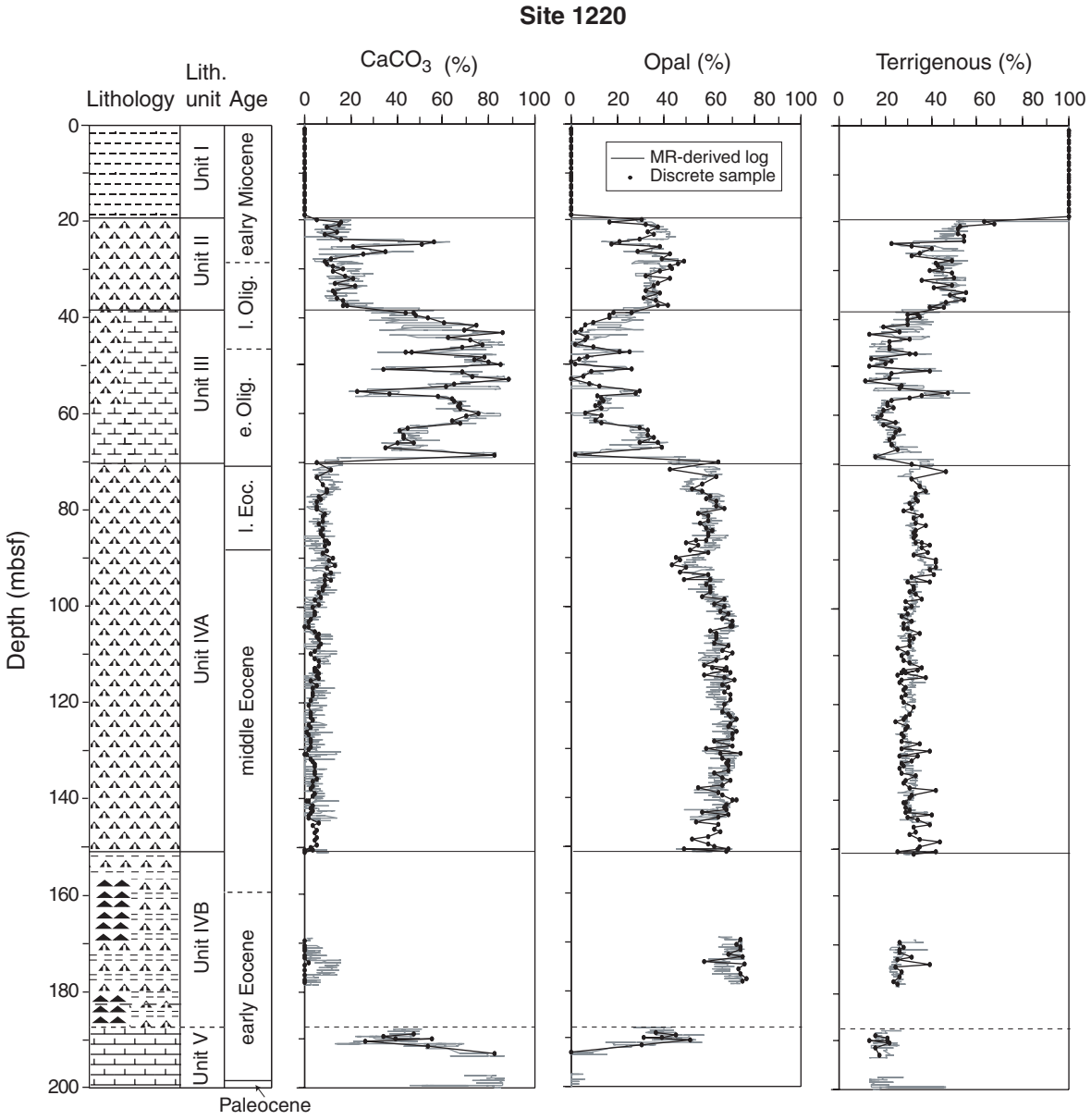

Figure F3 (continued).

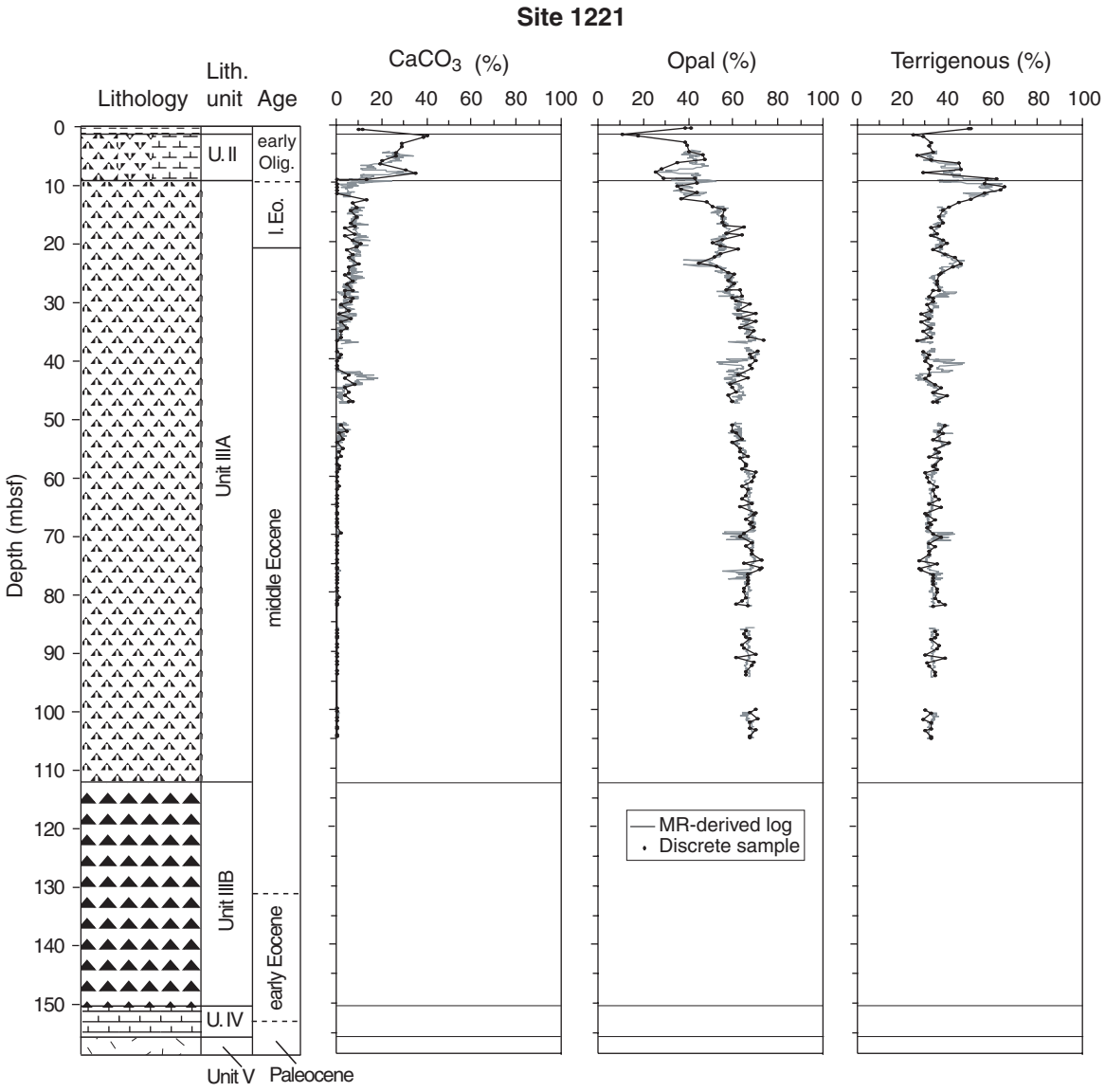

Figure F3 (continued).

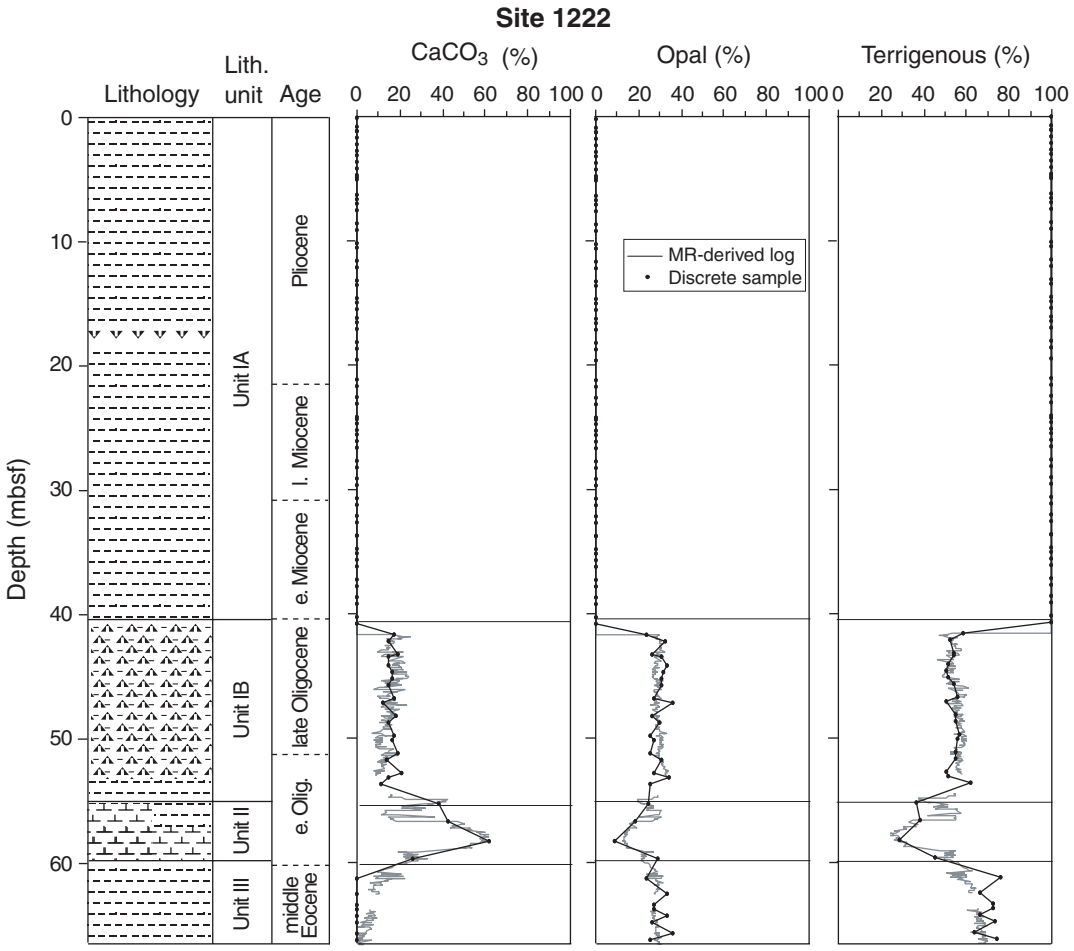

Figure F4. Downcore changes in VNIS-based clay mineralogy for the upper clay units of sites drilled during Leg 199. Sites are arranged from north (left) to south (right). Available paleomagnetic reversal data are also included to the right of the appropriate graph.

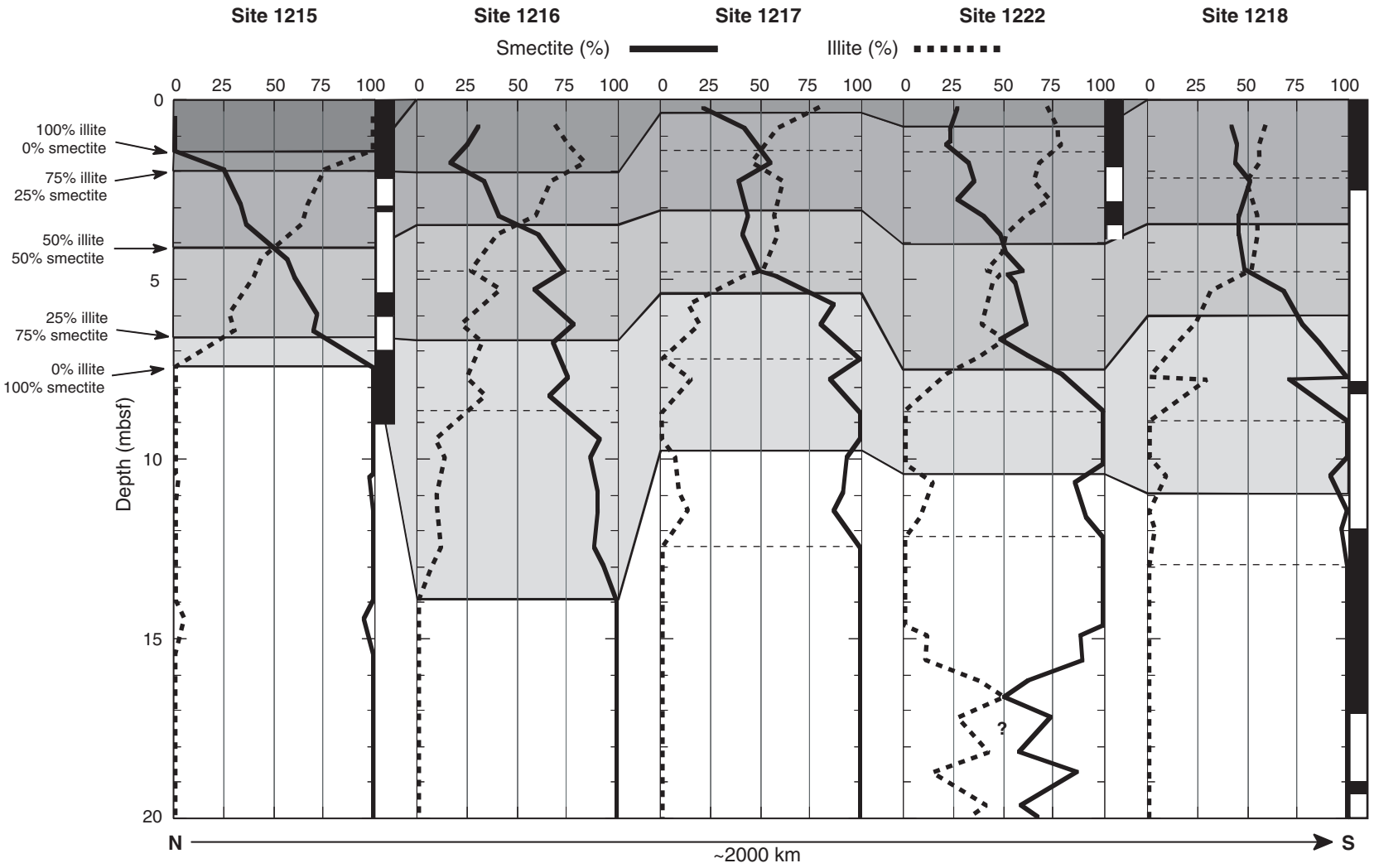

Figure F5. Visible and near-infrared spectroscopy (VNIS)-based calcite concentrations compared with calcite concentrations measured by coulometer for Leg 199 sites that contain calcite.

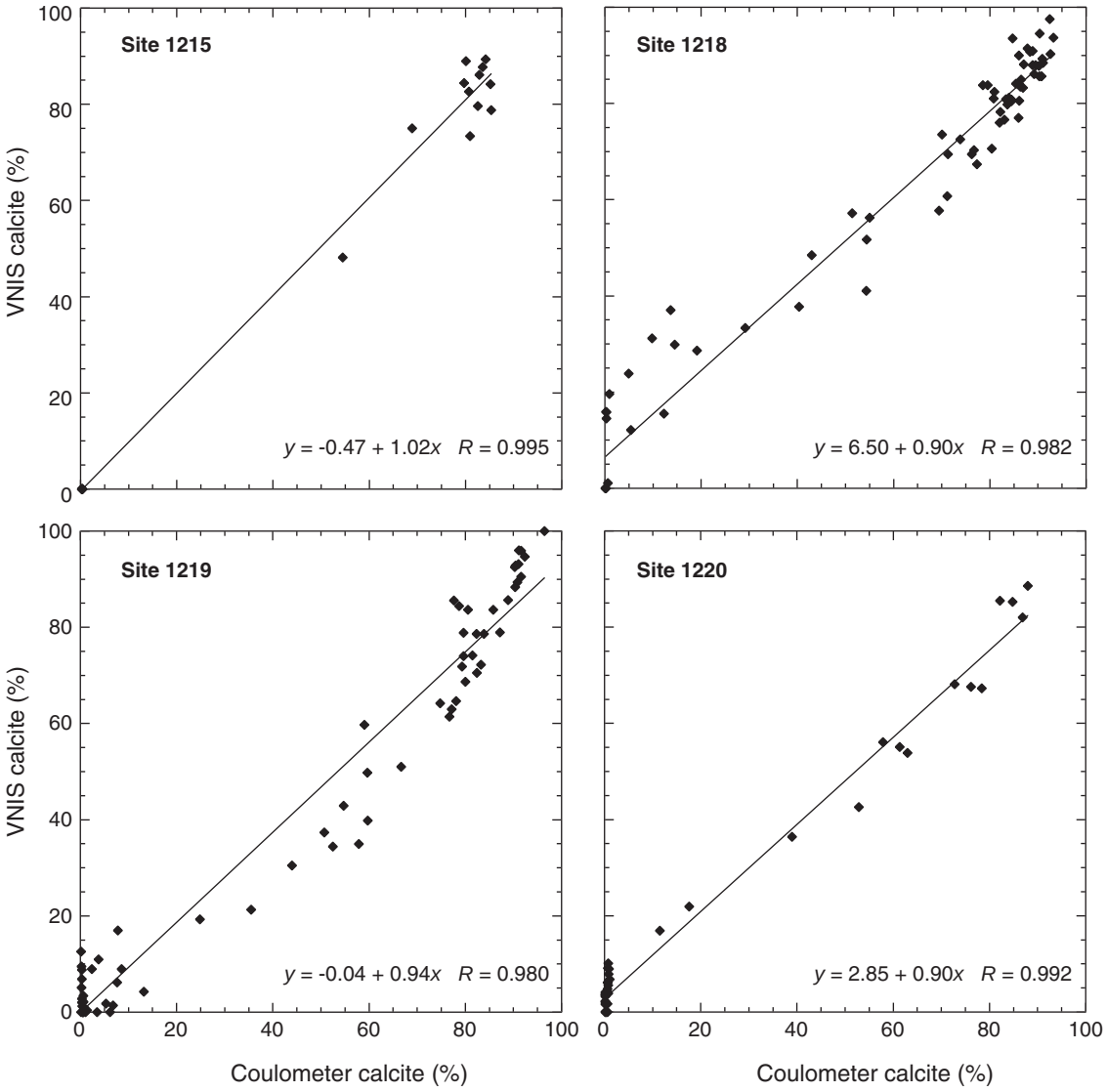

Table T1. Mineralogical ground-truth data used to calibrate VNIS spectral features for postcruise analysis. (See table notes. Continued on next page.)

Core, section, interval (cm)	Calcite (%)		Opal (%)		Smectite (%)		Illite (%)	
	Ground-truth	VNIS	Ground-truth	VNIS	Ground-truth	VNIS	Ground-truth	VNIS
199-1215A-								
1H-1, 49–51	0.00	0.00	0.00	0.00	0.00	6.82	100.00	93.18
2H-1, 23–25	0.00	0.00	0.00	0.00	0.00	6.95	100.00	93.05
2H-1, 75–77	0.00	0.00	0.00	0.00	0.00	0.00	100.00	100.00
4H-5, 75–77	54.50	48.23	0.00	0.00	45.50	51.77	0.00	0.00
5H-5, 75–77	80.15	89.00	0.00	0.00	19.85	11.00	0.00	0.00
9H-2, 84–86	68.93	75.05	0.00	1.76	31.07	23.19	0.00	0.00
199-1218A-								
16H-6, 81–83	93.18	93.20	0.00	0.00	6.82	6.80	0.00	0.00
17H-6, 75–77	92.47	97.49	0.00	0.00	7.53	2.51	0.00	0.00
19H-2, 75–77	92.65	90.32	0.00	0.00	7.35	9.68	0.00	0.00
199-1219A-								
12H-4, 69–71	92.36	94.68	0.00	0.00	7.64	5.32	0.00	0.00
13H-4, 75–77	91.62	89.64	0.00	2.39	8.38	7.96	0.00	0.00
EW97909 site survey cores								
3PC (PAT-13), 33–35	0.22	0.00	12.00	0.00	0.00	12.53	87.78	87.47
3PC (PAT-13), 314–316	0.04	7.74	15.50	23.73	84.46	68.53	0.00	0.00
3PC (PAT-13), 433–435	0.14	2.33	20.70	27.56	79.16	70.11	0.00	0.00
3PC (PAT-13), 773–775	0.12	0.00	52.60	53.44	47.28	46.56	0.00	0.00
3PC (PAT-13), 830–832	0.33	0.00	60.90	59.04	38.77	40.96	0.00	0.00
3PC (PAT-13), 933–935	0.09	0.00	57.90	56.54	42.01	43.46	0.00	0.00
3PC (PAT-13), 1192–1194	0.09	0.00	55.90	55.67	44.01	44.33	0.00	0.00
3PC (PAT-13), 1337–1339	0.08	0.00	57.00	58.32	42.92	41.68	0.00	0.00
7PC (PAT-8), 122–124	0.16	1.87	17.70	21.96	82.14	76.17	0.00	0.00
7PC (PAT-8), 335–337	0.30	0.00	24.70	25.08	75.00	74.92	0.00	0.00
7PC (PAT-8), 387–389	0.31	0.00	22.20	20.72	77.49	79.28	0.00	0.00
7PC (PAT-8), 518–520	0.33	0.00	20.60	18.75	79.07	81.25	0.00	0.00
7PC (PAT-8), 696–698	0.34	10.08	32.10	25.41	67.56	64.51	0.00	0.00
7PC (PAT-8), 804–806	52.46	43.39	14.40	15.87	33.14	40.74	0.00	0.00
7PC (PAT-8), 829–831	67.50	56.96	8.90	9.22	23.60	33.82	0.00	0.00
7PC (PAT-8), 982–984	0.36	10.70	34.60	26.02	65.04	63.28	0.00	0.00
7PC (PAT-8), 1163–1165	0.31	9.86	31.90	33.15	67.79	56.99	0.00	0.00
7PC (PAT-8), 1252–1254	0.26	7.40	29.70	27.21	70.04	65.38	0.00	0.00
7PC (PAT-8), 1317–1319	16.45	19.09	24.90	23.27	58.65	57.64	0.00	0.00
7PC (PAT-8), 1367–1369	17.24	20.69	31.70	23.13	51.06	56.18	0.00	0.00
7PC (PAT-8), 1436–1438	30.35	26.90	24.00	23.35	45.65	49.75	0.00	0.00
7PC (PAT-8), 1466–1468	27.04	30.41	22.20	20.94	50.76	48.65	0.00	0.00
7PC (PAT-8), 1518–1520	78.91	74.85	7.00	3.11	14.09	22.04	0.00	0.00
12PC (PAT-17), 258–260	0.18	6.76	36.30	31.97	63.52	61.27	0.00	0.00
12PC (PAT-17), 473–475	43.67	32.94	22.90	30.05	33.43	37.01	0.00	0.00
12PC (PAT-17), 593–595	36.53	41.68	26.10	23.89	37.37	34.43	0.00	0.00
12PC (PAT-17), 740–742	0.29	7.36	42.50	41.32	57.21	51.32	0.00	0.00
12PC (PAT-17), 833–835	0.22	7.44	50.80	45.38	48.98	47.18	0.00	0.00
12PC (PAT-17), 979–981	0.14	6.83	37.30	39.75	62.56	53.42	0.00	0.00
12PC (PAT-17), 1074–1076	0.03	6.75	45.80	43.89	54.17	49.36	0.00	0.00
12PC (PAT-17), 1261–1263	63.63	58.34	15.10	17.68	21.27	23.99	0.00	0.00
21GC (PAT-15), 20–22	0.37	0.00	10.60	0.00	0.00	0.00	89.03	100.00
21GC (PAT-15), 115–117	0.11	0.00	9.30	0.00	0.00	0.00	90.59	100.00
21GC (PAT-15), 175–177	0.07	0.00	10.60	0.00	0.00	0.10	89.33	99.90
21GC (PAT-15), 235–237	0.04	0.00	12.20	0.00	0.00	20.70	87.76	79.30
16-162-								
1R-1, 91–92	51.68	34.88	15.08	24.03	33.24	41.09	0.00	0.00
1R-2, 61–62	46.94	36.34	18.39	23.45	34.67	40.21	0.00	0.00
1R-3, 80–81	60.02	33.92	7.79	21.75	32.19	44.32	0.00	0.00
3R-2, 80–81	72.33	65.44	10.90	10.86	16.77	23.70	0.00	0.00
3R-3, 80–81	67.64	58.35	10.32	14.67	22.04	26.97	0.00	0.00
3R-4, 80–81	77.60	68.64	7.32	10.21	15.08	21.15	0.00	0.00
3R-5, 70–71	57.34	79.72	6.50	5.39	36.16	14.88	0.00	0.00
4R-3, 79–80	3.97	4.81	43.43	37.85	52.60	57.33	0.00	0.00
4R-4, 80–81	3.56	13.91	45.26	38.51	51.18	47.57	0.00	0.00
4R-5, 77–78	3.14	10.05	48.89	52.40	47.97	37.55	0.00	0.00
4R-6, 60–61	5.96	8.46	54.27	52.15	39.77	39.39	0.00	0.00
14R-2, 80–81	16.03	25.21	52.02	39.58	31.95	35.21	0.00	0.00

Table T1 (continued).

Core, section, interval (cm)	Calcite (%)		Opal (%)		Smectite (%)		Illite (%)	
	Ground-truth	VNIS	Ground-truth	VNIS	Ground-truth	VNIS	Ground-truth	VNIS
14R-3, 81–82	28.66	17.89	42.15	41.67	29.19	40.43	0.00	0.00
14R-4, 80–81	35.26	28.91	37.14	39.07	27.60	32.02	0.00	0.00

Notes: VNIS-predicted mineral percentages for each ground-truth sample are also shown. Calcite percentages for Sites 1215, 1218, and 1219 are from Lyle, Wilson, Janecek, et al. (2002). Clay was found by subtracting percent calcite from 100%. Opal was assumed to be negligible. The dominant clay mineral (smectite or illite) was identified from VNIS spectra. Data from site survey cores and Leg 162 are from Olivarez-Lyle and Lyle (2002).

Table T2. Spectral features used in the postcruise mineralogy calculation.

Mineral	Significant spectral features	Regression coefficient	Correlation coefficient	Constant
Clay solution:				
Illite	(2208 nm – 2500 nm)/TR1	–18.09	0.992	37.22
	SQR(TR)	–14.48		
	[(2200 nm trough – 1900 nm trough)/TR]$^{0.6}$	–22.44		
Smectite	[(2200 nm trough – 1900 nm trough)/TR]$^{0.6}$	36.20	0.977	43.69
Three-mineral solution:				
Calcite	[(1400 nm trough depth)/TR]$^{0.65}$	–6.09	0.964	31.42
	[(2260 nm peak – 2330 nm trough)/TR]$^{0.6}$	4.52		
	(2383 nm – 2336 nm)/TR	25.36		
Opal	(1900 nm trough depth)/TR	17.23	0.969	25.83
	[(2260 nm peak – 2330 nm trough)/TR]$^{0.6}$	–12.37		
	(2267 nm + 2323 nm – 2248 nm – 2296 nm)/TR	–9.08		
Smectite	SQR(TR)	–4.85	0.953	42.75
	[(2260 nm peak – 2330 nm trough)/TR]$^{0.6}$	5.41		
	(2383 nm – 2336 nm)/TR	–30.61		
	[(2200 nm trough – 1900 nm trough)/TR]$^{0.6}$	–15.03		

Note: TR = average reflectance over the entire measured bandwidth (350–2500 nm).

Table T3. Multiple regression analyses to convert the continuous MST/Minolta logs into mineralogy logs.

Site	Mineral component	Depth interval (mcd)	R^2	Logs used	Regression coefficient	Constant
1215	$CaCO_3$	26.44–67.48	0.92	Den, MS, Ref, a*	47.546, –0.360, 1.174, 2.452	–50.412
	Terrigenous	26.44–67.48	0.92	Den, MS, Ref, a*	–51.177, 0.310, –1.115, –1.746	149.214
1216						
1217	$CaCO_3$	26.76–128.88	0.89	Den, MS, Ref, a*, b*	51.832, –0.396, 1.349, –7.836, 4.648	–73.501
	Opal	26.76–128.88	0.96	MS, Ref, b*, a*/b*	–0.735, –1.528, 1.473, 88.579	39.914
	Terrigenous	26.76–128.88	0.98	Den, MS, b*	–31.761, 1.167, –0.609	52.020
1218	$CaCO_3$	34.94–187.46	0.98	Den, MS, Ref, a*, a*/b*	64.052, –0.820, –0.260, 3.012, –85.817	21.178
	$CaCO_3$	196.14–242.04	0.95	Den, MS	81.376, –0.429	–50.185
	$CaCO_3$	242.5–273.76	0.98	Den	156.649	–180.819
	Opal	34.94–187.46	0.91	Den, a*, b*, a*/b*	–24.420, 6.366, –2.548, –34.255	60.877
	Opal	196.14–242.04	0.8	Den	–42.311	75.617
	Opal	242.5–273.76	0.96	Den, a*/b*	–140.799, –27.216	239.107
	Terrigenous	34.94–273.76	0.94	Den, MS, Ref, b*	–55.460, 0.739, 0.270, –0.551	82.570
1219	$CaCO_3$	0.75–99.76	0.98	Den, MS, b*	123.063, –0.445, 1.389	–124.041
	$CaCO_3$	100.66–244.39	0.98	Den, Ref, a*	122.891, 0.313, –1.826	–146.357
	Opal	0.75–99.76	0.93	Den, Ref, a*/b*	–67.245, 0.212, 44.037	81.839
	Opal	100.66–206.75	0.98	Den, MS, Ref, a*	–95.284, –0.784, –0.483, 1.280	203.647
	Opal	207.24–244.39	0.99	Den, MS, b*	–94.301, 0.097, 0.748	169.153
	Terrigenous	0.75–20.24	0.91	Den, Ref, a*, b*, a*/b*	271.108, –1.716, –26.128, 14.601, 139.030	–264.864
	Terrigenous	20.76–152.6	0.89	Den, MS, b*, a*/b*	–13.383, 0.490, –0.602, 25.503	36.495
	Terrigenous	154.1–244.39	0.95	Den, MS, a*/b*	–50.275, 0.371, –5.382	88.899
1220	$CaCO_3$	19.8–68.76	0.98	Den, Ref, b*	141.444, 0.330, 4.419	–172.938
	$CaCO_3$	70.26–192.95	0.91	Den, MS, Ref	65.502, 0.279, 1.166	–112.882
	Opal	19.8–68.76	0.93	Den, MS	–118.118, –0.847	186.957
	Opal	70.26–192.95	0.88	Den, MS, Ref, b*	–67.338, –0.761, –0.827, 0.908	174.463
	Terrigenous	19.8–68.76	0.95	Den, MS, Ref, a*/b*	–29.327, 0.447, –0.687, 1.485	80.568
	Terrigenous	70.26–192.95	0.78	Den, MS, Ref, a*/b*	–13.814, 0.475, –0.294, 0.365	46.539
1221	$CaCO_3$	4.74–55.24	0.81	MS, a*, a*/b*	–0.259, –3.566, –71.118	84.932
	$CaCO_3$	55.76–104.42	0.49	Den, MS	–2.520, 0.059	2.109
	Opal	4.74–13.26	0.62	Den	–160.672	222.434
	Opal	14.24–82.02	0.82	MS	–0.761	75.324
	Opal	86.28–104.42	0.49	Den	38.847	24.556
	Terrigenous	4.74–104.42	0.89	Den, MS	–18.040, 0.465	46.382
1222	$CaCO_3$	41.64–66.16	0.76	Ref, b*	0.955, 3.384	–44.853
	Opal	41.64–66.16	0.54	Ref, a*	–0.451, –2.378	53.642
	Terrigenous	41.64–66.16	0.87	Ref, a*/b*	–0.512, 69.291	37.160

Notes: Den = GRA bulk density, MS = magnetic susceptibility, Ref = average reflectance over entire visible range (*L), a* = reflectance in the red region, b* = reflectance in the blue region; a*/b* = ratio of red to blue wavelengths. Regression coefficients correspond to logs. Site 1216 contains only terrigenous minerals.